ChemComm

COMMUNICATION

Highly efficient and durable PtCo alloy nanoparticles encapsulated in carbon nanofibers for electrochemical hydrogen generation†

TingTing Yang, Han Zhu, Meng Wan, Liang Dong, Ming Zhang and MingLiang Du*

Cite this: *Chem. Commun.*, 2016, 52, 990

Received 28th September 2015,
Accepted 6th November 2015

DOI: 10.1039/c5cc08097e

www.rsc.org/chemcomm

PtCo/CNFs exhibit extraordinary catalytic activity and durability for hydrogen evolution reaction, even approaching the performance of the commercial Pt/C catalyst, which can be attributed to the alloy structure and the encapsulation of PtCo alloy nanoparticles in CNFs.

Hydrogen is proposed as a promising clean and renewable energy source to meet the increasing energy and environmental demands.[1,2] Water electrolysis has been widely investigated as a highly important method for hydrogen generation through the hydrogen evolution reaction (HER). Notwithstanding the tremendous efforts that have been made to find alternative materials, it must be pointed that platinum (Pt) still plays an irreplaceable role in the HER due to its high catalytic activity. However, the prohibitive cost and scarcity of Pt limit its practical applications.[1] Toward this end, decreasing Pt usage is always the ultimate goal for electrocatalyst design to achieve cost-effective hydrogen production; meanwhile, HER catalysts with long term stability and high activity are also urgently needed.[1,3]

In this regard, a way to solve these problems is to make a Pt alloy with a 3d transition metal (such as cobalt, nickel and iron) because this new type of material exhibits unusual properties[4] together with high stability,[5] and it is expected to have enhanced catalytic activity due to the modification of the Pt electronic structure (the correlation of the ligand and strain effects for example).[6,7] Generally, the PtCo alloy demonstrates superior activity to pure Pt and excellent electrochemical self-stability toward the oxygen reduction reaction (ORR).[8,9]

The preparation of metal nanoparticles (NPs) encapsulated in carbon nanofibers (CNFs) can efficiently confine the NPs' size and prevent agglomeration during the catalytic process.[10,11] It should be mentioned that the interconnected 3D architecture of the CNF network is regarded as an ideal support material, which can enable rapid electron transport and fast gas diffusion, providing large interfaces and interstices between the catalytically active sites and the electrolyte.[12]

Herein, with respect to the catalytic activity and strong durability of the PtCo alloy in ORR and the advantage of CNFs as a catalyst support material, we proposed a facile strategy for fabricating PtCo alloy NPs encapsulated in carbon nanofibers (PtCo/CNFs) by integrating the electrospinning and graphitization processes. After graphitization, uniform PtCo alloy NPs were formed *in situ* and encapsulated in the matrix of CNFs. Encouraged by the above-mentioned promising findings, we then further evaluated the HER catalytic performance of PtCo/CNFs. Surprisingly, the PtCo/CNFs (with a Pt content of *ca.* 5 wt%) exhibit amazing catalytic activity and cyclic performance, which even approaches that of the commercial Pt/C (20 wt%) catalyst. Therefore, the present investigation may provide a fundamental insight into designing new structures with high catalytic performance, especially for HER.

The morphology of PtCo/CNFs was determined by field-emission scanning electron microscopy (FESEM, Fig. 1a) and transmission electron microscopy (TEM, Fig. 1d and e), which clearly disclosed that PtCo alloy NPs were homogeneously dispersed in the CNFs with diameters of *ca.* 10.9 nm and without any aggregation. Likewise, the Pt NPs and Co NPs were evenly grown on the surface of CNFs (Fig. 1b and c), respectively. The high-resolution TEM (HRTEM) micrograph (Fig. 1f) presents a crystalline PtCo alloy, and it clearly identifies that the *d*-spacings for NPs are 0.229 and 0.262 nm corresponding to the (111) and (200) planes of face-centered cubic (fcc) crystals,[13] respectively, indicating the formation of the PtCo alloy.

The high-angle annular dark-field scanning transmission electron microscopy (HAADF-STEM) observations are also consistent with the uniform dispersion of PtCo alloy NPs due to the space-confined growth (Fig. 2a).[14] Additionally, elemental mapping further evidenced the formation of the PtCo/CNFs (Fig. 2b), in which both the carbon and nitrogen species were evenly distributed throughout the nanocomposites, while Pt and Co were homogeneously overlaid in individual NPs with no

Department of Materials Engineering, College of Materials and Textile, Zhejiang Sci-Tech University, Hangzhou 310018, P. R. China.
E-mail: du@zstu.edu.cn; Tel: +86-0571-86843255

† Electronic supplementary information (ESI) available. See DOI: 10.1039/c5cc08097e

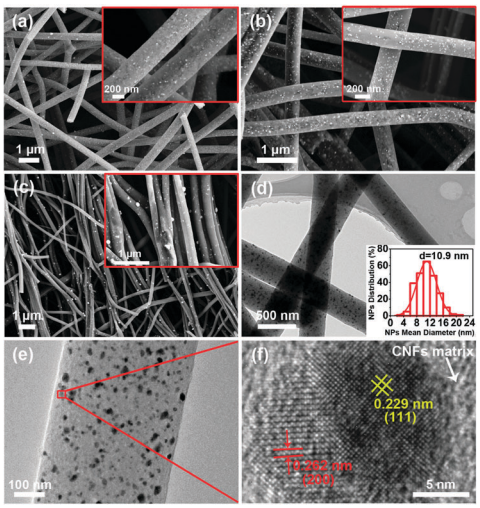

Fig. 1 (a–c) FESEM images of PtCo/CNFs, Pt/CNFs and Co/CNFs. (d and e) TEM images of PtCo/CNFs. The inset in (d) shows the corresponding average diameter of PtCo alloy NPs within the CNFs. (f) HRTEM image of a PtCo nanocrystal in the CNFs.

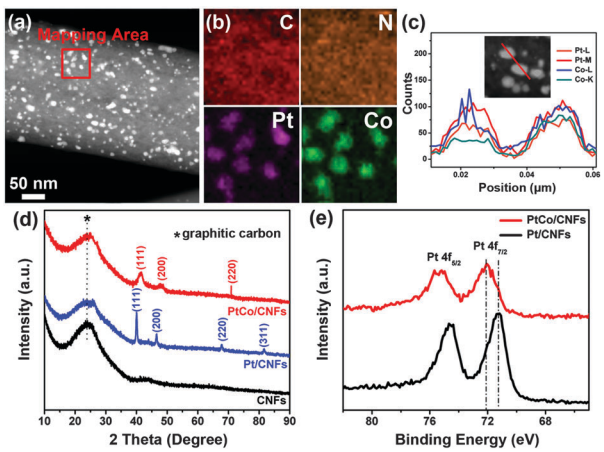

Fig. 2 (a) HAADF-STEM image and (b) STEM-EDS mapping images of the PtCo/CNFs. (c) Line scan EDX spectra of PtCo alloy NPs encapsulated in CNFs. (d) XRD patterns of CNFs, Pt/CNFs and PtCo/CNFs. (e) Pt 4f XPS spectra of the Pt/CNFs and PtCo/CNFs.

obvious phase segregation. Furthermore, as illustrated in Fig. 2c, the chemical composition of the NPs was also probed with the assistance of line-scan energy dispersive X-ray (EDX) analysis over two NPs, which displayed the relative intensities of the Pt and Co elements, confirming the successful fabrication of the PtCo alloy with a Pt : Co molar ratio of 1 : 0.78.

As depicted in Fig. 2d, the X-ray diffraction (XRD) pattern of CNFs exhibits a characteristic (002) plane peak for graphite (JCPDS 75-1621) at approximately 23.5°, demonstrating the crystalline structure of graphitic carbon in CNFs. For Pt/CNFs, the diffraction peaks are consistent with the standard pattern of fcc crystalline Pt (JCPDS, 04-0802). It is interesting to note that the diffraction peaks of PtCo/CNFs shift slightly toward higher angles compared to those of the Pt/CNFs. Meanwhile, the three diffraction peaks appearing at 41.5° (111), 47.6° (200) and 69.9° (220) are consistent with those of the PtCo alloy with a fcc structure, pointing out a lattice contraction arising from the partial substitution of Pt atoms by Co atoms to form an alloy phase.[5,9,15]

XPS was further used to verify the formation of the PtCo alloy. For PtCo/CNFs, two obvious peaks at 72.0 and 75.1 eV (Fig. 2e) are ascribed to Pt $4f_{7/2}$ and Pt $4f_{5/2}$, respectively. Strikingly, compared to 71.4 and 74.5 eV that are expected for pure Pt in Pt/CNFs, the Pt 4f peaks of PtCo/CNFs are shifted to higher energies upon alloy formation with Co, which is in line with the reported theory.[16] Meanwhile, the upward shift of the core level of the PtCo alloy is due to the charge transfer from Co to Pt atoms.[3,17]

To decode the electrochemical performance of PtCo/CNFs (with Pt and Co content of *ca.* 5 and 2.4 wt%, respectively) toward HER, linear sweep voltammetry (LSV) was performed in oxygen-free 0.5 M H_2SO_4 solution. As a control, similar measurements for the commercial Pt/C catalyst (Johnson-Matthey, 20 wt%), CNFs, Pt/CNFs (*ca.* 8.5 wt% Pt) and Co/CNFs (*ca.* 5.3 wt% Co) were also tested. As expected, the commercial Pt/C catalyst exhibits extraordinarily high HER activity with a near zero onset overpotential *versus* the reversible hydrogen electrode (RHE) (Fig. 3a). Interestingly, the onset overpotential of PtCo/CNFs is close to that of commercial Pt/C, indicating that the PtCo alloy can significantly improve the catalytic activity. Furthermore, PtCo/CNFs afford a current density of 10.0 mA cm^{-2} at −63 mV, which is very near to that of commercial Pt/C (about −57 mV) and much lower than those of Pt/CNFs and Co/CNFs at −104 mV and −475 mV, respectively. In addition, PtCo/CNFs exhibit much higher mass activity than Pt/CNFs and Co/CNFs (Fig. S1, ESI†), which also demonstrates the extraordinary electrocatalytic activity of the PtCo/CNFs.

A small Tafel slope of a catalyst is desirable for practical applications because it leads to a strongly enhanced HER rate at a moderate overpotential increase, which is an inherent property of electrocatalysts.[18] As shown in Fig. 3b, Tafel plots derived from the polarization curves were constructed. Again, the as-synthesized PtCo/CNFs exhibit an extraordinary low Tafel slope, even identical to that of commercial Pt/C (28 mV dec^{-1}), which is quite lower than those of Pt/CNFs (40 mV dec^{-1}), Co/CNFs (109 mV dec^{-1}) and CNFs (135 mV dec^{-1}), further indicating its favorable reaction kinetics (see Fig. 3b).[19] Then, electrochemical impedance spectra (EIS) measurements were also performed at −0.25 V *vs.* RHE, as presented in Fig. 3c. The charge-transfer resistance (R_{ct}) is related to the electrocatalytic kinetics and, clearly, the lower R_{ct} of PtCo/CNFs suggests a faster HER kinetics at higher overpotential.

As is well known, the commercial Pt/C catalyst exhibits a very high HER activity and is the most efficient HER catalyst. However, in the present investigations as described above, the synthesized PtCo/CNFs catalyst with a Pt content of *ca.* 5 wt% exhibits extraordinary high HER activity, which is quite close to that of commercial Pt/C (20 wt%). The extraordinary high catalytic performance of the PtCo/CNFs could be rationalized as follows: (1) the incorporation of Co into a PtCo alloy helps to maintain free and active Pt sites for electrocatalytic reactions due to a bifunctional mechanism.[20] (2) The interconnected 3D

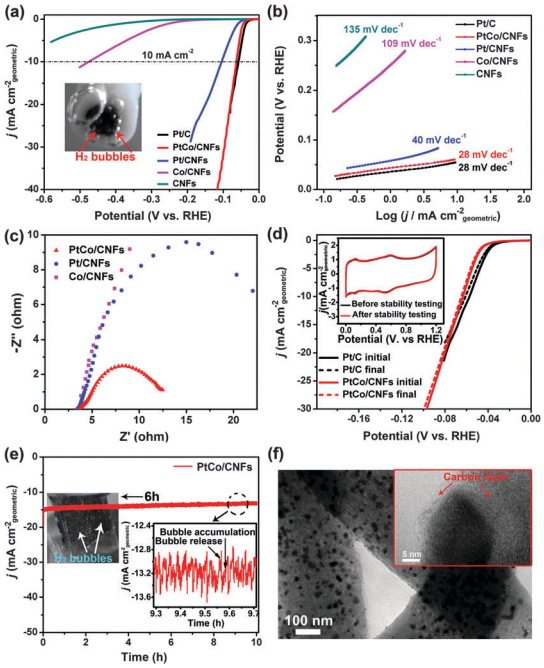

Fig. 3 (a) Polarization curves and (b) Tafel plots of CNFs, Co/CNFs, Pt/CNFs, commercial Pt/C (Johnson-Matthey, 20 wt%) and PtCo/CNFs (scan rate: 2 mV s^{-1}). Inset in (a): optical image of PtCo/CNFs coated on a glassy-carbon electrode (GCE) operating at 50 mV with generated bubbles on the surface suggesting the formation of H_2 gas. (c) Electrochemical impedance spectra (EIS) were recorded in the frequency range from 100 kHz to 0.1 Hz with an amplitude of 10 mV at −0.25 V *vs.* RHE. (d) Polarization curves of PtCo/CNFs and the commercial Pt/C catalyst before and after 1000 potential cycles (scan rate: 100 mV s^{-1}). Inset shows CV curves of PtCo/CNFs before and after potential cycles. (e) Chrono-amperometric response (*j*–*t*) recorded for a PtCo/CNFs membrane which was cut into a neat square (1 × 1 cm) at a constant applied potential of −0.056 V *vs.* RHE. The PtCo/CNFs membrane catalyst was directly used as the working electrode. Inset in panel e: digital photo of the H_2 bubbles formed on the PtCo/CNFs membrane at a time point of 6 h, and the enlargement of the area is denoted by a dashed circle. (f) TEM images of PtCo/CNFs after stability testing with the inset showing the HRTEM image. All of the measurements were performed in an Ar-saturated 0.5 M H_2SO_4 solution.

architecture of the CNF network can enable rapid electron transport and fast gas diffusion because CNFs provide a large area of electrolyte/nanofiber interfaces and interstices between the fibers.[12,21]

Apart from having a high catalytic activity, the long term durability of a catalyst electrode toward HER is another critical requirement for energy conversion and storage systems, especially for practical applications.[22] After 1000 cycles at a scan rate of 100 mV s^{-1} between 0 and 1.2 V *vs.* RHE, the polarization curve of PtCo/CNFs was still the same as the initial one, and only a negligible cathodic current density loss was observed (Fig. 3d). In addition, as shown in the inset of Fig. 3d, the PtCo/CNFs electrode showed no obvious decrease in the CV curve after 1000 potential cycles. To further investigate the practical applications in electrocatalytic water splitting, the PtCo/CNFs membrane was directly used as a working electrode. It can be observed that the corresponding current density of the PtCo/CNFs membrane was observed with no distinct degradation after 10 h of testing (Fig. 3e), and the alternate processes of bubble accumulation and bubble release can be confirmed by the serrate shape of the current (inset Fig. 3e). Moreover, the surface structure of PtCo/CNFs remained the same as the original morphology, and no aggregation or detachment of the PtCo alloy NPs was observed after potential testing (Fig. 3f and Fig. S2, ESI†). These suggest that the PtCo/CNFs are even more stable than commercial Pt/C under HER conditions.

Co species have generally been regarded as unstable catalysts in acidic solution, restricting their application in HER. However, we found that PtCo/CNFs exhibited excellent stability, which was even greater than that of commercial Pt/C in the present investigation. Such a high stability of PtCo/CNFs is ascribed to the effective suppression of the Ostwald ripening effect when Co is incorporated into the crystal lattice of Pt.[6,23] Furthermore, as the PtCo alloy NPs are encapsulated in the carbon layers (inset, Fig. 3f), the carbon layer will protect the PtCo alloy NPs from erosion by the electrolyte and prevent PtCo alloy NPs from detaching and coalescing,[10,14] resulting in high long term stability.

With the introduction of Co, we synthesized a PtCo/CNFs catalyst with extraordinary high HER activity and much lower Pt content. However, some concerns, such as the relationship between the PtCo ratio and the HER activity, the optimal composition of the alloy, and the HER activity in comparison with PtCo/C and commercial Pt/C, are still not quite certain. In our future work, these concerns will be explored and expected to be fully resolved.

In summary, we reported an effective hydrogen evolution catalyst PtCo/CNFs, which can be made by the combination of electrospinning and carbonization processes. The PtCo/CNFs catalyst exhibits an extraordinary high HER activity and strong durability. The PtCo/CNFs nanocomposites with a low Pt loading content (*ca.* 5 wt%) afforded a small overpotential and a small Tafel slope of merely 28 mV dec^{-1}, which approached that of the commercial Pt/C catalyst (20 wt%). The PtCo/CNFs catalyst also competes with commercial Pt/C (20 wt%) with regard to its excellent stability, which can be attributed to the alloy structure and the encapsulation of PtCo alloy NPs in CNFs. It is anticipated that PtCo/CNFs may improve the HER activity and lower the cost, which is promising for water-splitting devices and other generic key renewable energy systems.

This study was supported by the National Natural Science Foundation of China (NSFC) (Grant no. 51373154, 51573166), the Program for Innovative Research Team of Zhejiang Sci-Tech University and the 521 Talent Project of Zhejiang Sci-Tech University.

Notes and references

1 S. Bai, C. M. Wang, M. S. Deng, M. Gong, Y. Bai, J. Jiang and Y. J. Xiong, *Angew. Chem., Int. Ed.*, 2014, **53**, 12120–12124.
2 W. J. Zhou, K. Zhou, D. M. Hou, X. J. Liu, G. Q. Li, Y. H. Sang, H. Liu, L. G. Li and S. W. Chen, *ACS Appl. Mater. Interfaces*, 2014, **6**, 21534–21540.
3 S. L. Choi, S. U. Lee, W. Y. Kim, R. Choi, K. Hong, K. M. Nam, S. W. Han and J. T. Park, *ACS Appl. Mater. Interfaces*, 2012, **4**, 6228–6234.
4 V. R. Stamenkovic, B. Fowler, B. S. Mun, G. F. Wang, P. N. Ross, C. A. Lucas and N. M. Markovic, *Science*, 2007, **315**, 493–497.

5 Q. Sun, S. G. Wang and R. M. Wang, *J. Phys. Chem. C*, 2012, **116**, 5352–5357.
6 J. F. Xu, X. Y. Liu, Y. Chen, Y. M. Zhou, T. H. Lu and Y. W. Tang, *J. Mater. Chem.*, 2012, **22**, 23659–23667.
7 R. Loukrakpam, J. Luo, T. He, Y. S. Chen, Z. C. Xu, P. N. Njoki, B. N. Wanjala, B. Fang, D. Mott, J. Yin, J. Klar, B. Powell and C. J. Zhong, *J. Phys. Chem. C*, 2011, **115**, 1682–1694.
8 S. Hidaia, M. Kobayashia, H. Niwaa, Y. Haradaa, M. Oshimaa, Y. Nakamorib and T. Aoki, *J. Power Sources*, 2011, **196**, 8340–8345.
9 D. L. Wang, H. L. L. Xin, R. Hovden, H. S. Wang, Y. C. Yu, D. A. Muller, F. J. DiSalvo and H. D. Abruña, *Nat. Mater.*, 2013, **12**, 81–87.
10 T. T. Yang, M. L. Du, H. Zhu, M. Zhang and M. L. Zou, *Electrochim. Acta*, 2015, **167**, 48–54.
11 Y. H. Su, Y. H. Zhu, H. L. Jiang, J. H. Shen, X. L. Yang, W. J. Zou, J. D. Chen and C. Z. Li, *Nanoscale*, 2014, **6**, 15080–15089.
12 B. Li, X. M. Ge, F. W. T. Goh, T. S. A. Hor, D. S. Geng, G. J. Du, Z. L. Liu, J. Zhang, X. G. Liu and Y. Zong, *Nanoscale*, 2015, **7**, 1830–1838.
13 Z. F. Hu and J. C. Yu, *J. Mater. Chem. A*, 2013, **1**, 12221–12228.
14 H. Zhu, M. L. Du, M. Zhang, M. L. Zou, T. T. Yang, S. L. Wang, J. M. Yao and B. C. Guo, *Chem. Commun.*, 2014, **50**, 15435–15438.
15 W. F. Huang, Q. Zhang, D. F. Zhang, J. Zhou, C. Si, L. Guo, W. S. Chu and Z. Y. Wu, *J. Phys. Chem. C*, 2013, **117**, 6872–6879.
16 Y. Vasquez, A. K. Sra and R. E. Schaak, *J. Am. Chem. Soc.*, 2005, **127**, 12504–12505.
17 M. Wakisaka, S. Mitsui, Y. Hirose, K. Kawashima, H. Uchida and M. Watanabe, *J. Phys. Chem. B*, 2006, **110**, 23489–23496.
18 D. Merki and X. L. Hu, *Energy Environ. Sci.*, 2011, **4**, 3878–3888.
19 W. J. Zhou, D. M. Hou, Y. H. Sang, S. H. Yao, J. Zhou, G. Q. Li, L. G. Li, H. Liu and S. W. Chen, *J. Mater. Chem. A*, 2014, **2**, 11358–11364.
20 D. Liu, Q. H. Guo, H. Q. Hou, O. Niwa and T. Y. You, *ACS Catal.*, 2014, **4**, 1825–1829.
21 H. L. Fei, Y. Yang, Z. W. Peng, G. D. Ruan, Q. F. Zhong, L. Li, E. L. G. Samuel and J. M. Tour, *ACS Appl. Mater. Interfaces*, 2015, **7**, 8083–8087.
22 T. Y. Ma, S. Dai, M. Jaroniec and S. Z. Qiao, *J. Am. Chem. Soc.*, 2014, **136**, 13925–13931.
23 E. Antolini, J. R. C. Salgado and E. R. Gonzalez, *J. Power Sources*, 2006, **160**, 957–968.